Focussed on "Crack Paths"

Visual Abstract

The effect of creep damage model formulation on crack path prediction

Valery Shlyannikov, Andrey Tumanov
Institute of Power Engineering and Advanced Technologies, FRC Kazan Scientific Center, Russian Academy of Sciences, Russia.
shlyannikov@mail.ru, https://orcid.org/0000-0003-2468-9300
tymanoff@rambler.ru

ABSTRACT. The stress, strain rate and process zone with respect to the creep-crack growth are analyzed by employing damage-evolution equations. The damage models for the fracture of the process zone are represented using a stress and ductility based formulation. Special attention has been addressed in the present study to the influence of the creep damage model formulation on the crack path prediction. To evaluate the significance of dominating fracture mechanism a comparison of the cases for pure mode II is considered. It was observed that in the case of stress based model one side of the notch, dominated by tensile stresses, blunts, while the other side, dominated by shear strains, sharpens. In the case of ductility based model, there is a tendency for creep damage to localize only at the blunted part of the notch. This because the highest tensile hydrostatic stress and crack-tip constraint always occur near the blunted part of the notch. In this region, the crack growth direction and general creep damage zone deviate from the initial crack plane. As a result of numerical calculations the consequence of the crack deviation angle values, crack length increments and finally crack path were determined.

KEYWORDS. Creep damage; Limit stresses and strains; Crack path.

OPEN ACCESS

Citation: Shlyannikov V., Tumanov A., The effect of creep damage model formulation on crack path prediction, Frattura ed Integrità Strutturale, 48 (2019) 77-86.

Received: 03.12.2019
Accepted: 10.02.2019
Published: 01.04.2019

INTRODUCTION

In the past, the continuum damage mechanics (CDM) was used as a complementary approach in high-temperature fracture mechanics to analyze the damage and fracture process at different scales with respect to the changing material structure from the initiation of micro-cracks to the final fracture resulting from the macro-cracks [1, 2]. The CDM covered several microscopic mechanisms in the area near the macroscopic creep crack including void nucleation and growth on the grain-boundary facets, cavities coalescing to form a grain-size micro-crack, coalescing of micro-cracks, which finally lead to the propagation of creep macro-cracks.

In the present study the continuum damage mechanics is applied to assess the creep damage behavior. Special attention has been addressed to the influence of the creep damage model formulation on the on crack path prediction. To evaluate the significance of dominating fracture mechanism a comparison of the case for pure mode II is considered. The crack tip damage zones for extensive creep conditions are compared for stress and ductility based models. The crack growth direction and general creep damage zone deviate from the initial crack plane. As a result the consequence of the crack deviation angle values, crack length increments and finally crack path were determined.

STRESS BASED MODEL

Let ω denote in Eq.(1) the measure of damage with $\omega = 0$ denoting the undamaged state and $\omega = 1$ the fully damaged state. The creep strain rate accumulation constitutive equation is generalized by the authors [1, 2] to multi-axial state of stress using J_2 - flow theory as follows

$$\frac{d\varepsilon_{eqv}}{dt} = \frac{3}{2} B \sigma_{eqv}^{n-1} S_{ij} \left(\frac{1}{1-\omega} \right)^n \tag{1}$$

where B and n are constants of the Norton power law equation. The simplest creep damage rate model, which is introduced by Kachanov [1], is a function of applied nominal stress and current accumulated damage has the following form

$$\frac{d\omega}{dt} = C \left[\frac{\sigma_f^{(\pm)}}{(1-\omega)} \right]^m \tag{2}$$

where C and m are material constants. Similarly Eq.(2), Shlyannikov and Tumanov [3] introduced a model for the rate of accumulation of stress-based creep damage as a function of multi-axial stress function $\sigma_f^{(\pm)}$ described by Eqs.(3,4) in the generalized form

$$\sigma_f^{(\pm)} = (1-\chi)\sigma_{kk/mp}^{(\pm)} + \chi\sigma_e \tag{3}$$

$$\sigma_{kk} = \sigma_1 + \sigma_2 + \sigma_3 = 3\sigma_m, \quad \sigma_e = \left[\frac{3}{2} S_{ij} S_{ij} \right]^{1/2}, \quad S_{ij} = \sigma_{ij} - \sigma_m \delta_{ij}. \tag{4}$$

where χ is the experimental material constant that is determined as the ratio of uniaxial tensile to compression strength $\chi = \sigma_t / \sigma_c$. According to [16] the equivalent stresses can be present by the following equation

$$\sigma_{eqv} = (1-\chi)\sigma_1 + \chi\sigma_{\text{int}} \tag{5}$$

For $\chi = 0$ brittle fracture is occurred and the equivalent stresses corresponds to maximum tensile stresses (maximum tensile stress theory), while for ductile fracture $\chi = 1$ and $\sigma_{eqv} = \sigma_{\text{int}}$ (von Mises-Hencky's theory).

DUCTILITY BASED MODEL

The crack size is assumed to increase when the local accumulated creep strain at the crack tip reaches the critical creep ductility. In this case the damage evolution law is given by simple relationship

$$\dot{\omega} = \frac{d\omega}{dt} = \frac{\dot{\varepsilon}_{cr}}{\varepsilon_f^*}, \tag{6}$$

where $\dot{\omega}$ and $\dot{\varepsilon}_{cr}$ are the damage rate and the creep strain rate, respectively. Term ε_f^* denotes the multi-axial creep failure strain, which normally differs from the uniaxial creep ductility. Using the general critical-stress criterion in the form of Pisarenko-Lebedev [4] criterion, Shlyannikov [5] proposed a multi-axial failure strain equations:

$$\frac{\varepsilon_f^*}{\varepsilon_{f0}} = \left[\frac{1}{b_i} \left(\frac{\eta_i}{1-\chi+\chi\eta_i} \right)^n \right] \tag{7}$$

$$b_i = \frac{2}{3}\sqrt{1-\xi+\xi^2}\ ;\ \ \xi = \frac{\lambda\left(1-\nu^2\right)-\nu\left(1+\nu\right)}{\left(1-\nu^2\right)-\lambda\nu\left(1+\nu\right)};\ \ \eta_i = \sqrt{1-\lambda+\lambda^2+\nu\left(\nu-1\right)\left(1+\lambda\right)^2} \tag{8}$$

where ε_{f0} is uniaxial failure strain, $\lambda = \sigma_2/\sigma_1$ is the principal stress ratio, ν is Posson's ratio.

The basic relationship between the secondary creep rate $\dot{\varepsilon}_{cr}$ and creep rate in the tertiary range is given by Bendick [6]

$$\dot{\varepsilon} = \frac{\dot{\varepsilon}_{cr}}{\left(1-\omega\right)^g} \tag{9}$$

where $\dot{\varepsilon}_{cr} = B\sigma_e^n$ is modified Norton's law. Using this expression and substituting Eq.(9) into Eq.(6) one finds

$$\frac{d\omega}{dt} = \frac{\dot{\varepsilon}_{cr}}{\varepsilon_f^*(1-\omega)^m} = \frac{B\sigma_e^n}{\varepsilon_f^*\left(1-\omega\right)^g}\ . \tag{10}$$

For uniaxial tension Bendick [6] proposed relation between the secondary creep rate $\dot{\varepsilon}_{cr,0}$ and failure strain ε_{f0} based on the approximation of the experimental data for many different materials

$$\frac{\dot{\varepsilon}_{cr,0}t_f}{\varepsilon_{f0}} = \frac{B\sigma^n t_f}{\varepsilon_{f0}} = \alpha \quad \text{or} \quad \varepsilon_{f0} = \frac{B\sigma^n t_f}{\alpha} \tag{11}$$

where t_f is time to fracture and α is experimental constant. Substitution of Eqs. (7) and (8) into Eq. (10) leads to the expression for ductile creep damage rate under multi-axial stress-strain state

$$\frac{d\omega}{dt} = \frac{\alpha b_i \left[\left(1-\chi\right)/\eta_i+\chi\right]^n}{t_f}\left(\frac{\sigma_e}{\sigma}\right)^n \frac{1}{(1-\omega)^g} \tag{12}$$

Going back to Eq.(3) it should be noted that in Eq.(2) $d\omega/dt$ is assumed to be implicit function of the hydrostatic stress σ_m and the von Mises equivalent stress σ_e. The governing parameter in the form of the material constant χ helps in describing the effect of the multi-axial state of the stress-strain behavior of the material.

CRACK PATH PREDICTION PROCEDURE

Structural integrity prediction under mixed mode fracture generally includes two issues. The first is the crack path determination, while the second is the crack growth rate prediction along definite curvilinear trajectory. Crack path prediction for mixed mode loading carried out making use the following scheme (Fig.1). Crack was assumed to growth in a number of discrete steps. The principal feature of such modeling is determination of the crack growth direction and definition of crack length increment in this direction. After the crack is initiated with kinking, the stress and creep strain fields around the crack tip changes. In our computations the predicted initial crack angle θ_i coincides with the position of maximum value of the creep damage parameter ω (Eqs. (2) and (12)) after corresponding loading history. The virtual crack extension amount $\Delta a_i = (a_{i+1} - a_i)$ is the sum of linear sizes for FE number in which the creep damage exceed $\omega > 0.6$. Such finite elements are excluded from the global finite element mesh creating new free surfaces of the crack. The continuum damage formulation (Eqs.(1) and (6)) combined with the stress and ductility based models Eqs. (2) and (12) has been implemented in ANSYS via the user element subroutine.

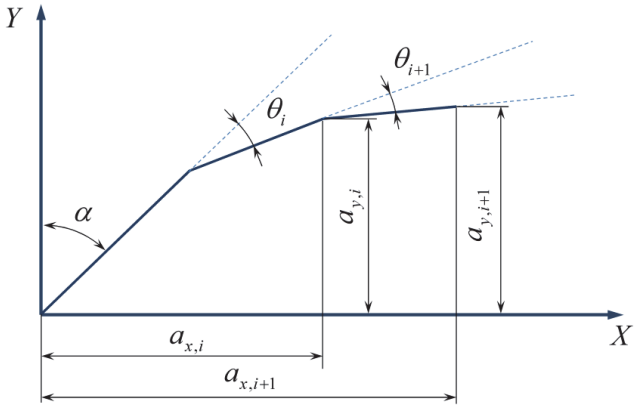

Figure 1: Crack path model.

RESULTS AND DISCUSSION

The geometry considered in this study is a biaxially loaded plate containing the inclined central crack (Fig.2,a). The panel is subjected to two perpendicular loads: one parallel to the y-axis σ and another parallel to the x-axis $\sigma\eta$. The combination of inclination crack angle α =45°and nominal stress biaxial ratio at equi-biaxial tension-compression η = -1 corresponds to pure mode II fracture. The center-cracked plate (CCP) contains an internal crack of length $2a$=20mm (a/w=0.01, where w is plate width) and loaded to a uniform biaxial stress of magnitude σ = 50 MPa. The 2D plane strain eight-node isoparametric elements were applied to CCP geometry. To consider the details of large deformation and blunting of the crack tip, a typical FE-mesh (Fig.2,b) was used with the initial notch root radius ρ/a =0.001. Computations were performed in ANSYS, in which the SOLID 186 element was employed, together with the user-defined creep damage law. We define the reference time t_T as the time corresponding to the transition from the small-scale creep to the extensive creep conditions. The considered material is power steam turbine rotor steel R2M. The creep properties of analyzed material at the elevated temperature of 550°C are summarized in Table 1. In our case the transition time for given nominal stress σ =50 MPa and crack length a =10mm is t_T = 21.88 hrs.

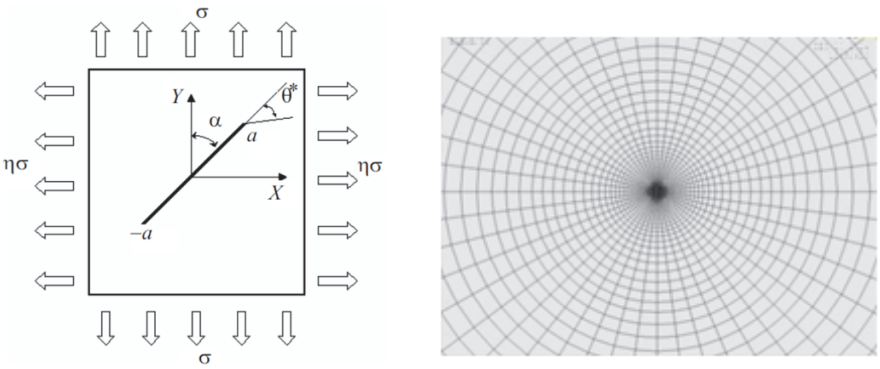

a) b)

Figure 2: Biaxially loaded plate with inclined crack.

E [GPa]	ν	σ_0 [MPa]	B [1/(MPa^n·hr)]	n	C [1/(MPa^m·hr)]	m	g
200	0.3	100	1×10^{-14}	5.0	1×10^{-10}	3.0	5.0

Table 1: The creep properties of material.

A fracture-damage zone (FDZ) or fracture-process zone (FPZ) local with respect to the crack tip is defined as the core where the microstructure damage accumulates until the crack growth occurs at the macroscopic scale level. After

determining these stress invariants in the FEM procedure, the creep-damage distribution or the FPZ shape and size are obtained by integrating Eqs.(2) and (11) for stress and ductility models, respectively. The crack tip damage zones under pure mode II for extensive creep conditions t/t_T=45.7 are shown in Fig.3 for stress (a) and ductility (b) based models.

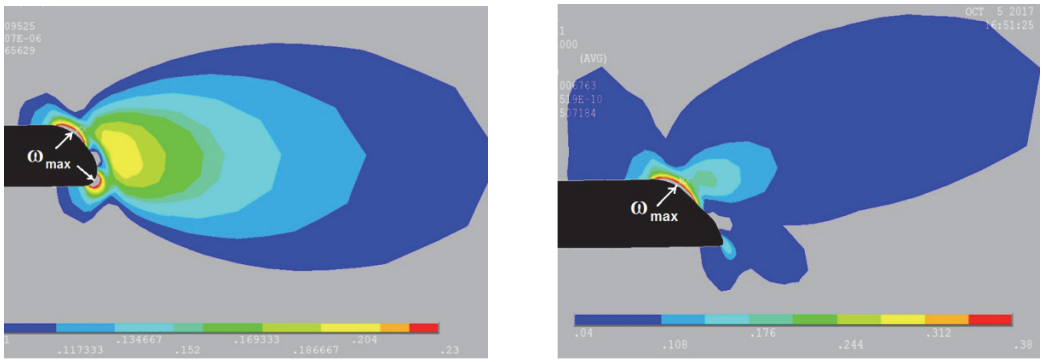

a) b)

Figure 3: Mode II crack tip creep damage zones for stress (a, χ=1.0) and ductility (b, χ=0.6) models at t/t_T=45.7.

It can be observed in Fig. 3 non-uniform deformation and damage fields near an initially smooth notch tip under mode II loading conditions. In the case of stress based model (Fig.3,a) one side of the notch, dominated by tensile stresses, blunts, while the other side, dominated by shear strains, sharpens. Thus, two competing fracture mechanisms occur at the blunted and the sharpened part of the notch respectively. As the result the general creep damage zone is approximately symmetrical with respect to the initial crack plane. In the contrary, in the case of ductility based model (Fig.3,b), there is a tendency for creep damage to localize only at the blunted part of the notch. This because the highest tensile hydrostatic stress and crack-tip constraint always occur near the blunted part of the notch. In this region, crack initiation and propagation takes place due to microvoid coalescence. The crack growth direction and general creep damage zone in Fig.3,b deviate from the initial crack plane.

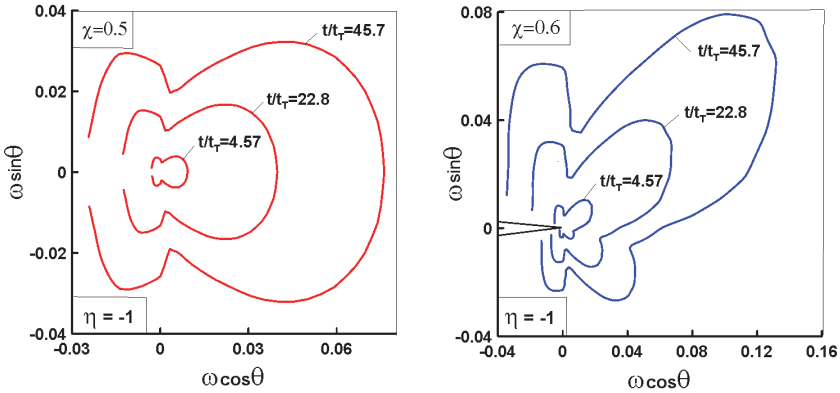

a) b)

Figure 4: Creep damage zone as a function of creep time for (a) stress and (b) ductility based models.

The contours, shown in Fig. 4, demonstrated the process of the crack-tip stress and ductility damage accumulation under the biaxial loading as a function of the creep time. The finite element calculations have been presented for material cases wherein the multi-axial stress formulation (Eqs. (5) and (6)) is a function of the hydrostatic or principal stresses. Note that, stress (a) and ductility (b) based creep damage contours do not coincide with each other at the same creep time. Based on the comparison the stress and ductility creep damage models for pure mode II, it can be seen that at equibiaxial tension-compression $\eta = -1.0$ in Fig.4(a) for the stress model, the maximum distance of the damage contour boundary from the crack tip is located along the crack line for any creep time. However in Fig.4(b) for the ductility model, the maximum size of the creep-damage zone deviated sufficiently from the crack line to directly ahead of the crack tip (0 °direction) as a function of the multi-axial stress material constant χ.

CREEP CRACK PATH PREDICTION

By employing the constitutive Eq. (1), as well as damage models Eqs.(2) and (12) directly into the FEM rate-dependent formulation and using an explicit time integration procedure, we obtain a standard Runge–Kutta integration scheme wherein the finite-element stiffness matrix is derived from the elastic moduli. Thus, to determine the numerical stress/strain-rate fields, we need to first determine the damage-rate function by substituting the stress obtained in the initial iteration into Eqs.(2) and (12) for stress and ductility based models, respectively. After determining the damage function ω using numerical integration and by substituting the creep strain rate $\dot{\varepsilon}_{ij}$ of Eq. (1) obtained from the resulting damage function ω into the ANSYS, the damage stress/strain rate fields are found. Finally, after obtaining the solution to the nonlinear problem, the ANSYS output file is used as an input data for the special code developed to determine the dimensionless stress-strain angular distributions, damage contour, and creep-stress intensity factor.

We shall remind that on the plate containing the inclined central crack (Fig.2,a) subjected to biaxial tension-compression loads the pure Mode II takes place when the load biaxiality ratio is η = -1 and α =45°. Fig. 5 shows several computational crack paths as a function of the creep holding time. It is evident that, the crack propagates no longer in the initial direction. From comparison of our computations for pure Mode II obtained on both the compact tension-shear and cruciform specimens with appropriate experimental data [7] which was obtained using the steel and aluminum alloy follows that the crack initiation directions predicted from the numerical prediction and analytical solution are in good agreement. As is seen in Fig.5, inclusion in Eqs.(2) and (12) the creep damage functions allows one to take into account the influence constitutive equation formulation on a creep crack path prediction.

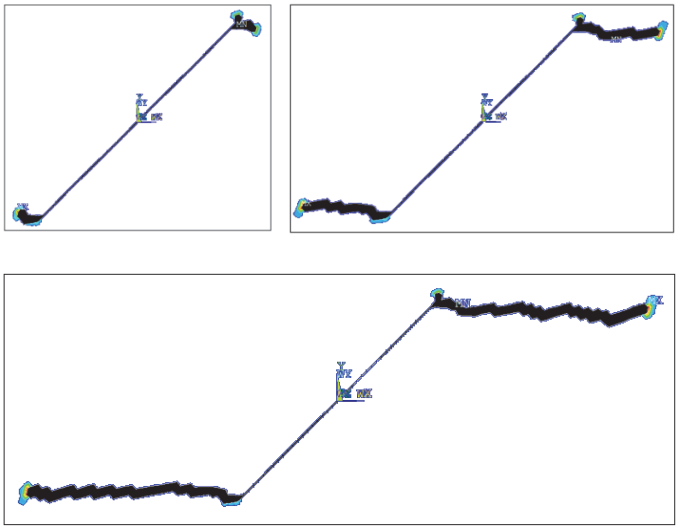

Figure 5: Creep crack path prediction for pure mode II.

Considering the crack-growth interpretation, in particularly creep crack path prediction, it should be noted that the effect of the creep-damage accumulation on the creep-crack growth rate might be scaled through the corresponding value of the creep-stress intensity factor (SIF) introduced by the authors [8, 9]. In addition, an inherent property of the creep SIF is the dependence on the multi-axial stress state through the equation for the damage functions (Eqs. 3 and 7). Furthermore, current value of the creep SIF is sensitive to the class of using creep damage models, i.e. stress or ductility based models.

CREEP STRESS INTENSITY FACTOR

According to approach [8] K_{σ} is amplitude of singularity in the form of creep stress intensity factor. For extensive creep conditions the relation between the C-integral and creep SIF is introduced by the authors [8] as follows:

$$\bar{K}_{cr}=\frac{1}{\sigma_0}\left(\frac{C^*}{BI_n^{cr}L}\right)^{\frac{1}{n_{cr}+1}} \tag{13}$$

$$C^*=\left(\bar{K}_{cr}\sigma_0\right)^{n_{cr}+1}\left(BI_n^{cr}L\right) \tag{14}$$

where C^* is the C-integral. The value of this line integral corresponding secondary creep deformation used in [10] as the relevant loading parameter to characterize the local stress-strain rate fields at any instant around the crack front in a cracked body subjected to extensive creep conditions

$$C^*=\int_{\Gamma}\left(\dot{W}dx_2-\sigma_{ij}n_j\frac{\partial\dot{u}_i}{\partial x_1}ds\right) \tag{15}$$

where the first term in Eq.(15) is the strain energy rate density (SERD) for power-law hardening creep [11,12]

$$\dot{W}_{cr}=\int_0^{\dot{\varepsilon}_{kl}}\sigma_{ij}^{cr}d\dot{\varepsilon}_{ij}^{cr}=\frac{n_{cr}}{n_{cr}+1}\sigma_e^{cr}\dot{\varepsilon}_e^{cr} \tag{16}$$

and Γ is an arbitrary counterclockwise path around the crack tip and the Cartesian coordinate system x_i is centered at the crack tip. Substitution of Eq. (16) into Eq. (15) leads to the expression for C^*-integral

$$C^*=\int_{-\pi}^{+\pi}Br\frac{n_{cr}}{n_{cr}+1}\left(\sigma_e^{cr}\right)^{n_{cr}+1}\cos\theta d\theta-\int_{-\pi}^{+\pi}\left[\sin\theta\left(\sigma_{rr}^{cr}\frac{\partial\dot{u}_r^{cr}}{\partial\theta}+\sigma_{r\theta}^{cr}\frac{\partial\dot{u}_\theta^{cr}}{\partial\theta}\right)-r\cos\theta\left(\sigma_{rr}^{cr}\frac{\partial\dot{u}_r^{cr}}{\partial r}+\sigma_{r\theta}^{cr}\frac{\partial\dot{u}_\theta^{cr}}{\partial r}\right)\right]d\theta \tag{17}$$

Similarly to the plastic problem, Eqn. (13) for the creep stress intensity factor include a governing parameter for power-law nonlinear viscous materials in the form of I_n^{cr}-integral which can be obtained using the numerical method elaborated by the authors [8]. This method was extended by Shlyannikov and Tumanov [13] to analyze the fracture resistance characteristics of creep-damaged material. According to this method, the I_n^{cr}-integral value can be determined directly from the FEA distributions of the displacement rate $\dot{\tilde{u}}_i^{cr}$ and dimensionless angular stress $\tilde{\sigma}_{ij}^{cr}$ functions

$$I_n^{cr}\left(\theta,t,n_{cr},\omega\right)=\int_{-\pi}^{+\pi}\Omega_{cr}^{FEM}\left(\theta,t,n_{cr},\omega\right)d\theta \tag{18}$$

$$\begin{aligned}\Omega_{cr}^{FEM}\left(\theta,t,n_{cr},\omega\right)=&\frac{n_{cr}}{n_{cr}+1}\left(\tilde{\sigma}_e^{cr}\right)^{n_{cr}+1}\cos\theta-\left[\tilde{\sigma}_{rr}^{cr}\left(\dot{u}_\theta^{cr}-\frac{d\dot{\tilde{u}}_r^{cr}}{d\theta}\right)-\tilde{\sigma}_{r\theta}^{cr}\left(\dot{u}_r^{cr}+\frac{d\dot{\tilde{u}}_\theta^{cr}}{d\theta}\right)\right]\sin\theta-\\&-\frac{1}{n_{cr}+1}\left(\tilde{\sigma}_{rr}^{cr}\dot{\tilde{u}}_r^{cr}+\tilde{\sigma}_{r\theta}^{cr}\dot{\tilde{u}}_\theta^{cr}\right)\cos\theta\end{aligned} \tag{19}$$

$$\dot{\tilde{u}}_i^{cr}=\frac{\dot{u}_i^{cr}}{BL\left(K_{cr}\right)^{n_{cr}}}\bar{r}^{\frac{n_{cr}}{n_{cr}+1}}=\frac{\dot{u}_i^{cr}\sigma_0^{n_{cr}}}{\dot{\varepsilon}_0L}\left(\frac{\tilde{\sigma}_e^{cr}}{\sigma_e^{cr}}\right)=\frac{\dot{u}_i^{cr}}{\dot{\varepsilon}_0L}\left(\frac{\tilde{\sigma}_e^{cr}}{\bar{\sigma}_e^{cr}}\right)^{n_{cr}}=\frac{du_i^{cr}}{dt}\frac{1}{\dot{\varepsilon}_0L}\left(\frac{\tilde{\sigma}_e^{cr}}{\bar{\sigma}_e^{cr}}\right)^{n_{cr}} \tag{20}$$

where t is creep time, $\tilde{\sigma}_e$ is the von Mises equivalent stress and $\bar{\sigma}_e^{cr}=\sigma_e^{cr}/\sigma_0$. In Eqs.(19,20) a dot over a displacement quantity denotes a time differentiations. The θ-variation angular functions of the suitably normalized functions $\tilde{\sigma}_{ij}$ and $\dot{\tilde{u}}_i$ and correspondingly governing parameter I_n^{cr}-integral depend on the damage function ω and creep exponent n. In the traditional models for creep or creep-fatigue crack growth rate prediction the I_n-integral is a function only the creep

exponent. In the present work it will be demonstrated that these governing parameters are different for elastic-plastic I_n^f and creep I_n^{cr} problems. Generally, they depend on the loading conditions including creep holding time and applied load, specified cracked body geometry, the elastic-plastic and creeping crack tip stress-strain fields, crack front curvature and size.

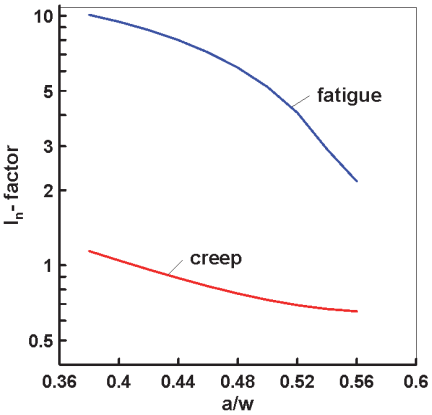

Figure 6: I_n-factor distributions for plastic and creep problems as a function of relative crack length.

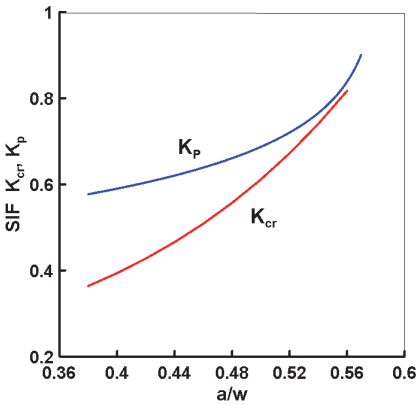

Figure 7: Plastic and creep SIFs behavior as a function of relative crack length.

Fig. 6 shows for the C(T) specimen the behavior of the governing parameter of elastic-plastic and creep crack-front fields in the form of the normalizing plastic and creep I_n-integrals (I_n^f, I_n^{cr}) as a function of relative crack length a/w at the mid-plane $z/b = 0.5$ and a crack front distance of $\overline{r} = 1.5 \cdot 10^{-3}$. It can be seen that the plastic and creep I_n-integral values do not coincide at the same loading conditions and crack length. Furthermore, in terms of the continuum damage mechanics formulation, as shown by the authors [13], the I_n^{cr}-integral distributions as functions of the creep times for undamaged and defective materials differ. Based on Eqs. (18-20), these distributions of the I_n-integral are used to calculate the plastic and creep SIFs in the C(T) specimen.

Fig. 7 illustrates the corresponding numerical results for the plastic and creep stress intensity factors behavior in the mid-plane of the C(T) specimen as a function of relative crack length. In this figure the finite element nonlinear SIFs variations correspond to the crack tip distance $\overline{r} = 1.384 \cdot 10^{-3}$. Fig. 7 shows the comparison of the plastic SIF behavior for power law cyclic strain hardening material and the creep SIF distribution for damaged elastic-nonlinear-viscous material with the damage parameter ω and constitutive law obtained using Eq. (12). As observed in Fig. 7, the plastic and creep SIF distributions as a function of relative crack length differ, and these distinctions depend on the number of loading cycles or creep time. Based on the comparison in Fig. 7, we can conclude that in the case of creep and fatigue interaction the dimensionless nonlinear stress intensity factors provide a more convenient representation of the fracture resistance characteristics of structural materials as parameters of the same scale.

In order to interpretation of test results and theoretical predictions for creep crack growth rate test results obtained on the C(T) specimen used C^*-integral and the creep stress intensity factor $\overline{K}_{cr}$ values based on experimentally determined force-line deflection (FLD) rate [14,15]

$$C^* = \frac{P\dot{V}_c}{b_s w}\left(\frac{f_g'}{f_g}\right) \tag{21}$$

$$\overline{K}_{cr} = \left[\frac{P}{BI_n^{cr}} \cdot \frac{\dot{V}_c}{b_s wL}\left(\frac{f_g'}{f_g}\right)\right]^{1/(n+1)} \tag{22}$$

where $\dot{V}_c$ - is the force-line displacement rate, f_g - is geometry dependent correction factor, $\left(f_g'\right)$ - is its derivative. In the case of theoretical prediction for creep crack growth rate in extensive creep conditions used the steady-state values of C^*-integral and corresponding expression for creep stress intensity factor $\overline{K}_{cr}$ for C(T) specimen in the following form [14,15]

$$C^* = B\left(w-a\right)h_1\left(\frac{P}{q\eta_1 b_s\left(w-a\right)}\right)^{\left(n_{cr}+1\right)} \tag{23}$$

$$\bar{K}_{cr} = \left[\frac{\left(w-a\right)h_1}{I_n^{cr}L}\right]^{\frac{1}{n_{cr}+1}}\left(\frac{P}{q\eta_1 b_s\left(w-a\right)\sigma_0}\right) \tag{24}$$

where $\eta_1 = \sqrt{\left(\frac{2a}{w-a}\right)^2 + 2\left(\frac{2a}{w-a}\right) + 2} - \left[\left(\frac{2a}{w-a}\right)+1\right]$; q = 1.455 - plane strain, q = 1.071- plane stress, h_1 is tabulated in Ref.[10].

In the general form, the creep SIF is a function of the cracked body configuration and their loading conditions, current crack length, holding time, damage, constraint parameters, and creep and multi-axial material properties. Under certain circumstances, this numerical solution may also have application to creeping solids that undergo damage near the crack tip. Thus, the creep SIF may by identified as a damage-sensitive high-temperature fracture parameter for correlating the crack growth under multi-axial stress/strain conditions. The fracture mechanics in terms of the creep-stress intensity factor provides a useful framework for correlating the data, for the design, and for remaining-life prediction.

CONCLUSIONS

The consequence of the crack deviation angle values, crack length increments and finally crack path were determined by local creep damage accumulation model. The effect of the creep-damage accumulation on the creep-crack growth rate might be scaled through the corresponding value of the creep-stress intensity factor. Thus, the creep SIF may by identified as a damage-sensitive high-temperature fracture parameter for correlating the crack growth under multi-axial stress/strain conditions.

ACKNOWLEDGMENT

The authors gratefully acknowledge the financial support of the Russian Science Foundation under the Project 17-19-01614.

REFERENCES

[1] Kachanov, L.M. (1986), Introduction to Continuum Damage Mechanics, Martinus-Nijhoff, Dordrecht.
[2] Lemaitre, J. (1996). A Course on Damage Mechanics, Springer-Verlag, Berlin, .
[3] Shlyannikov, V.N., Tumanov, A.V. (2018). Creep fracture resistance parameters determination based on stress and ductility damage model, Fatigue Fract. Eng. Mater. Struct., 41, pp. 2110-2129.
[4] Pisarenko, G.S., Lebedev, A.A. (1976). Deformation and Strength of Materials under Complex State of Stress, Naukova Dumka, Kiev.
[5] Shlyannikov, V.N. (2003). Elastic-Plastic Mixed-Mode Fracture Criteria and Parameters, Springer Verlag, Berlin, .
[6] Bendick, W. (1991). Analysis of material exhaustion and damage by creep, Int. J. Pres. Vess. Piping, 47, pp. 57–78.
[7] Shlyannikov, V.N., Tumanov, A.V. (2014). Characterization of crack tip stress fields in test specimens using mode mixity parameters, Int. J. Fract. 185, pp. 49–76.
[8] Shlyannikov, V.N., Tumanov, A.V., Boychenko, N.V. (2015). A creep stress intensity factor approach to creep-fatigue crack growth, Engng. Fract. Mech. 142, pp. 201–219.
[9] Shlyannikov, V.N., Tumanov, A.V., Boychenko, N.V., Tartygasheva, A.M. (2016). Loading history effect on creep-fatigue crack growth in pipe bend, Int. J. Press. Vess. Piping 139-140, pp. 86–95.
[10] Saxena, A. (1998). Nonlinear fracture mechanics for engineers. CRC Press LCC, 472p.
[11] Hutchinson, J.W. (1983). Constitutive behavior and crack tip fields for materials undergoing creep-constrained grain boundary cavitation, Acta Metall, 31, pp. 1079-1088.

[12] Yun-Jae, K. (2001). Contour integral calculations for generalized creep laws within ABAQUS, Int J Press Vess Piping. 78, pp. 661-666.
[13] Shlyannikov, V.N., Tumanov, A.V. (2018). Creep damage and stress intensity factor assessment for plane multi-axial and three-dimensional problems, Int. J. Solids Struct. 150, pp. 166–183.
[14] Shlyannikov, V.N., Tumanov, A.V., Boychenko, N.V. (2018). Creep-fatigue crack growth rate assessment using ductility damage model, Int. J. Fatigue 116, pp. 448–461.
[15] ASTM E2760–10, (2010). Standard test method for creep-fatigue crack growth testing. Annual book of ASTM standards. Philadelphia (PA): American Society for Testing and Materials.
[16] Pisarenko, G.S. and Lebedev, A.A. (1976). Deformation and Strength of Materials at Complex Stressed State [in Russian], Naukova Dumka, Kiev .